



HAL
open science

Different roles of phosphorus in the nucleation of lithium aluminosilicate glasses

Pauline Glatz, Monique Comte, Laurent Cormier, Lionel Montagne, Bertrand
Doumert, Galan G. Moore

► **To cite this version:**

Pauline Glatz, Monique Comte, Laurent Cormier, Lionel Montagne, Bertrand Doumert, et al.. Different roles of phosphorus in the nucleation of lithium aluminosilicate glasses. *Journal of Non-Crystalline Solids*, 2018, 493, pp.48-56. 10.1016/j.jnoncrysol.2018.04.021 . hal-02624877

HAL Id: hal-02624877

<https://hal.inrae.fr/hal-02624877v1>

Submitted on 5 Dec 2023

HAL is a multi-disciplinary open access archive for the deposit and dissemination of scientific research documents, whether they are published or not. The documents may come from teaching and research institutions in France or abroad, or from public or private research centers.

L'archive ouverte pluridisciplinaire **HAL**, est destinée au dépôt et à la diffusion de documents scientifiques de niveau recherche, publiés ou non, émanant des établissements d'enseignement et de recherche français ou étrangers, des laboratoires publics ou privés.

Different roles of phosphorous in the nucleation of lithium aluminosilicate glasses

Pauline Glatz^{a,b,c,*}, Monique Comte^a, Laurent Cormier^b, Lionel Montagne^c, Bertrand Doumert^d, Galan G. Moore^e

^aCorning European Technology Center, 7 Bis Avenue de Valvins, 77210 Avon-France

^bSorbonne Université, CNRS, Museum National d'Histoire Naturelle, IRD, Institut de Minéralogie, de Physique des Matériaux et de Cosmochimie (IMPMC), UMR 7590, 4 place Jussieu, 75005 Paris, France

^cUniv. Lille, CNRS, Centrale Lille, ENSCL, Univ. Artois, UMR 8181 - UCCS - Unité de Catalyse et Chimie du Solide, F-59000 Lille, France

^dUniv. Lille, CNRS, INRA, Centrale Lille, ENSCL, Univ. Artois, FR 2638 - IMEC - Institut Michel-Eugène Chevreul, F-59000 Lille, France

^eCorning Incorporated, Corning, New York 14831, USA

Abstract

Glasses in the $\text{Li}_2\text{O}-\text{Al}_2\text{O}_3-\text{SiO}_2$ (LAS) system with different $\frac{\text{Al}_2\text{O}_3}{\text{Li}_2\text{O}}$ ratio with or without addition of P_2O_5 have been synthesized and characterized by thermal analysis. The glass structure and the phosphorous environments in the glasses and their evolutions with annealing have been studied by ^{31}P Solid-State Nuclear Magnetic Resonance (SSNMR) and $31\text{P}/27\text{Al}$ D-HMQC (Dipolar Hetero-nuclear Multiple-Quantum Coherence) correlation NMR. The crystallization behavior has been studied by XRD, SSNMR and RAMAN spectroscopy. The results showed a different role for P_2O_5 depending on the $\frac{\text{Al}_2\text{O}_3}{\text{Li}_2\text{O}}$ ratio. For low alumina content, P_2O_5 plays a nucleating role while it acts as crystallization inhibitor for high alumina content. These different roles are related to different local environments of the phosphorus in the as-cast glasses. Our study emphasizes the importance of POAl complexes in the crystallization process of aluminosilicate glasses.

Keywords: P_2O_5 , Glass structure, Glass-ceramics, Thermal Analysis, NMR spectroscopy

* Author to whom correspondence should be addressed. e-mail: pauline.glatz@upmc.fr

1. Introduction

Glass-ceramics are materials obtained by controlled crystallization of glasses, which is achieved by thermal heat treatment on parent glasses. [1] The lithium aluminum silicate (LAS) ternary system is one of the most studied and a large number of materials with this composition are commercialized due to their excellent thermo-physical properties. As typical examples we can mention: the near-zero thermal expansion property for β -quartz solid solution glass-ceramics used for telescope mirror, stove cooktops and firedoor applications [2, 3], or the good mechanical properties for compositions with low amount of Al_2O_3 used in the field of restorative dentistry [4]. Since the properties of the glass-ceramics are widely dependent of the nature and relative amount of crystalline phases, the control of nucleation is a key step in order to optimize the final properties. To promote bulk crystallization and obtained an uniform distribution of crystals in the material, nucleating agents such as TiO_2 , ZrO_2 , and P_2O_5 are typically added in the $\text{Li}_2\text{O}-\text{Al}_2\text{O}_3-\text{SiO}_2$ (LAS) glass composition. [5, 6, 7]. In particular, phosphorous, which is classified as a typical network former in glasses, has a complex structural role that strongly impacts its solution behavior, the melt viscosity [8] or its ability to promote liquid-liquid phase separation and affect the crystallization mechanisms [9].

In a study on the effect of the $\frac{\text{Al}_2\text{O}_3}{\text{M}_2\text{O}}$ ratio (where $\text{M}=\text{Li,Na}$) on the crystallization of LAS system with P_2O_5 addition [10], different crystalline phases were reported depending on the Al_2O_3 content and volume crystallization was observed at low Al_2O_3 amount contrary to surface crystallization observed at high alumina content. Indeed, P_2O_5 is a well-known nucleating agent for low alumina LAS compositions, yielding to $\text{Li}_2\text{Si}_2\text{O}_5$ crystallization. [5, 11, 12, 13, 14] In terms of nucleation mechanism, Headley and Loehman [15] reported that lithium orthophosphate Li_3PO_4 crystals act as heterogeneous nuclei for silicate crystalline phases (metasilicate Li_2SiO_3 and disilicate $\text{Li}_2\text{Si}_2\text{O}_5$ phases). Successive studies using solid state ^{31}P MAS-NMR gave insight on the changes around phosphorous occurring during the crystallization processes [16, 17, 18].

Indeed, MAS-NMR techniques probe the local environment around phosphorus and reveal modifications occurring in the first crystallization steps which could conceivably be missed by other techniques [19]. On a disilicate (aluminum-free) glass-ceramic composition, Holland et al [16] reported that crystalline Li_3PO_4 was not detected by MAS-NMR before the formation of $\text{Li}_2\text{Si}_2\text{O}_5$ phases. However, recent studies revealed that a highly disordered Li_3PO_4 phase is formed concomitantly with Li_2SiO_3 crystallization [17][18].

In aluminosilicate glasses, MAS-NMR showed that phosphorus has different environments depending on the $\frac{\text{Al}_2\text{O}_3}{\text{M}_2\text{O}}$ ratio [20][21]. At low P_2O_5 content, a majority of PO_4^{3-} orthophosphate and $\text{P}_2\text{O}_7^{4-}$ pyrophosphate groups are observed in the glass matrix, while for increasing Al_2O_3 contents, aluminophosphate groups are formed. Recent developments in NMR provide information on the connectivity of PO_4 tetrahedra with the aluminosilicate network. Spatial proximities between P and Al were reported in systems with low amount of P_2O_5 and Al_2O_3 [22][23] and aluminophosphate groups could be detected in such glasses. Nevertheless, such methods were not used up to now for the detailed study of the nucleation process by P_2O_5 in LAS glass-ceramics. The aim of the present work is to provide new insights to elucidate the role of phosphorous in crystallization mechanisms of LAS compositions with different $\frac{\text{Al}_2\text{O}_3}{\text{Li}_2\text{O}}$ ratio. We report a combination of characterization and spectroscopic methods to investigate the crystallization sequences and the nucleating role of phosphorous. NMR and Raman spectroscopies enable us to discuss the changes in the phosphorus environments in relation with the crystallization processes, showing a different behavior between the glasses containing low and high Al_2O_3 contents.

2. Experimental Section

2.1. Materials

Glasses were prepared in the $\text{Li}_2\text{O}-\text{Al}_2\text{O}_3-\text{SiO}_2$ (LAS) ternary system with addition of P_2O_5 oxide as a nucleating agent. Analytical grade precursors (Li_2CO_3 , Al_2O_3 , SiO_2 and $(\text{NH}_4)_2\text{HPO}_4$) were ground together, dried and

60 melted in a Pt crucible at 1550°C for 2 h, then quenched by immersing the
bottom of the crucible into water. The glasses were ground and molten once
again to ensure a good homogeneity. Table 1 reports the glass compositions.
They are located along the 74 mol% SiO₂ isopleth, with 0 or 1 mol% P₂O₅.
These compositions cover a range with a ratio $R = \frac{\text{Al}_2\text{O}_3}{\text{Li}_2\text{O}}$ from 0 (Al-free) to 1.3
65 (peraluminous composition). The glasses are labeled as follow: LASR-Pn, where
R is the ratio $\frac{\text{Al}_2\text{O}_3}{\text{Li}_2\text{O}}$ and n the mol% of P₂O₅. Transparent, bubble free, glasses
were obtained excepted for the LAS0-P1, which is opalescent. For all samples,
powder XRD patterns show the characteristic broad peak of amorphous materi-
als and no Bragg peak. The glass compositions were checked by Electron probe
70 micro-analyser (CAMPARIS, Paris, France) with a CAMECA SX-Five appara-
tus (15 kV, 10 nA) for SiO₂, Al₂O₃, P₂O₅ and by a Flame-Atomic Absorption
Spectrometer in emission mode (Agilent, AA280FS) for Li₂O content.

2.2. Differential scanning calorimetry

Differential Scanning Calorimetry (DSC) thermograms were recorded on a
75 404 C Pegasus calorimeter from Netzsch (Selb, Germany). All the measurements
were carried out in air and heat treatments were conducted at 10°C/min with a
bulk sample of ~50 mg in Pt crucible, using an empty Pt crucible as reference.
The crystallization temperature of the first exothermic event was determined
at the maximum of the peak. The glass transition temperatures T_g, the onset
80 crystallization temperatures T_x and the temperatures of the maximum of the
first crystallization peak T_c are reported in Table 1.

2.3. XRD

X-ray diffraction was carried out at room temperature using a diffractometer
(PANalytical X'Pert PRO) with Ni-filtered CuK α radiation ($\lambda = 1.5418 \text{ \AA}$). Data
85 were recorded in the $10^\circ \leq 2\theta \leq 80^\circ$ range with a step increment of 0.016° and an
interval time of 0.82 sec per step.

2.4. RAMAN spectroscopy

Raman spectra of the glasses and annealed glasses were obtained using a Horiba LabRam HR Evolution system with Ultra-Low Frequency (ULF) module, 1800 gr/mm grating, and a 532 nm laser operating at 100 mW. A x10 magnification objective was used for this study. Each sample was analyzed with an exposure time of 30 sec (per window) with 10 accumulations and a spectral window from 5 to 2000 cm^{-1} . No temperature correction nor normalization have been used for these spectra.

2.5. Scanning Electron Microscopy

Scanning Electron Microscopy (SEM) was used to observe the microstructure of the samples. Bulk glass pieces were embedded in epoxy resin, then cross sections were polished and etched with 1 mol% HF for 30 seconds. They have been coated with iridium (2 nm thick) and observed using a SEM-FEG (Field Emission Gun) ZEISS LEO 1550 (Jena, Germany), at a 5 kV accelerating voltage. Observations have been done with the In-lens secondary electrons detector.

2.6. Solid-state NMR

^{31}P and ^{27}Al MAS-NMR (Magic Angle Spinning Nuclear Magnetic Resonance) spectra were recorded at 9.4 and 18.8 T on Bruker AVANCE I and AVANCE III spectrometers, respectively, with a 4 mm probe at 12.5 kHz spinning speed for ^{31}P and a 3.2 mm probe at 20 kHz spinning speed for ^{27}Al . The Larmor frequencies were 161.9 and 208.5 MHz for ^{31}P and ^{27}Al , respectively. For ^{31}P , the pulse duration was $4.8 \mu\text{s}$ ($\pi/2$), and the recycle delay (rd) was 120 s. For ^{27}Al , the pulse duration was $1 \mu\text{s}$ ($\pi/10$), and the rd 2 s. The recycle delays have been defined to enable enough relaxation to get quantitative spectra. The ^{31}P chemical shifts are relative to 85% H_3PO_4 solution at 0 ppm and those of ^{27}Al are referred to $\text{Al}(\text{NO}_3)_3$ solution as 0 ppm. Decomposition of NMR spectra was done by using dmfit software[24]. The $^{27}\text{Al}/^{31}\text{P}$ 2D maps were edited with the dipolar heteronuclear multiple quantum coherence (D-HMQC)

sequence [22] on a 18.8 T spectrometer with a 3.2 mm HPA1 probe operating at a spinning frequency of 20 kHz. The 988×23 data points and 3988×19 for LAS0.2-P1 and LAS0.7-P1 samples, respectively, were acquired with a ^{27}Al selective $90^\circ\text{-}\tau\text{-}180^\circ\text{-}\tau$ spin-echo. The ^{31}P channel was irradiated with 90° pulses and with a 1.1 ms recoupling time with the SR4_1^2 sequence. Each t_1 was recorded with 16384 scans for LAS0.2-P1 (18432 for LAS0.7-P1) with a rd of 0.5 s.

3. Results

3.1. Study of the crystallization

3.1.1. DSC investigations

Figure 1 shows the DSC curves obtained during heating of the glasses with and without P_2O_5 and for different alumina contents. These curves show an endothermic shift of the baseline, which is characteristic of the glass transition (T_g). The increase in T_g when R ratio increases can be attributed to the polymerization of the aluminosilicate glass network. The crystallization of the glasses is revealed by exothermic peaks, which are more or less intense and broad as will be discussed hereafter. We observe two different crystallization behaviors depending on the R ratio: for low alumina content, $R < 0.7$, crystallization peaks are sharper and they appear at lower temperature in glasses with P_2O_5 than those without P_2O_5 . For the composition with $R = 0.2$, the DSC curve of the glass with P_2O_5 shows two crystallization peaks, located at 646°C and 740°C . These crystallization events are at lower temperatures compared to the glass without P_2O_5 , which exhibits a single crystallization peak at 770°C . These observations are consistent with those on other glasses from the literature, designed to form lithium disilicate glass-ceramics in the $\text{SiO}_2\text{-Al}_2\text{O}_3\text{-Li}_2\text{O-K}_2\text{O-ZrO}_2\text{-P}_2\text{O}_5$ system [11]. For $R \geq 0.7$, crystallization peaks are observed at higher temperatures for the glasses with P_2O_5 , compared to those without P_2O_5 . In addition, large crystallization exotherms (i.e. large ΔT , where ΔT is the width of the crystallization exotherm) are observed both with and without P_2O_5 . The complete attribution of the different exother-

mic events is beyond the scope of this paper. The parameter $\Delta T_x (=T_x - T_g)$, reflecting the glass stability (GS) [25], can also be considered. The higher the ΔT_x , the lower the ability of a glass to crystallize. In our case, the exact interpretation is not easy as two crystallization mechanisms can occur: volume crystallization and surface crystallization. However, a different behavior for the glasses containing P_2O_5 is clearly observable: when $R < 0.7$, ΔT_x is lower (lower GS) for compositions with P_2O_5 than ΔT_x for compositions without P_2O_5 . For $R \geq 0.7$, the opposite effect is observed: the addition of P_2O_5 increases the glass stability. As the role of P_2O_5 is different for low or high alumina content, we will focus our investigation on two glass compositions representative of these two different crystallization behaviors: the LAS0.2-P1 composition corresponding to $R < 0.7$ range and the LAS0.7-P1 composition corresponding to $R \geq 0.7$ range.

3.1.2. Crystalline phases detected by XRD and RAMAN analysis

The lack of Bragg peaks in the XRD pattern of the LAS0.2-P1 sample (figure 2a) confirms that the initial glass is amorphous. For the annealed samples, the first Bragg peaks are observed for a treatment at 650°C for 1 minute and are assigned to lithium metasilicate (Li_2SiO_3 , JCPDS No. 29-0829) and lithium disilicate ($\text{Li}_2\text{Si}_2\text{O}_5$, JCPDS No. 70-4856) phases. Then, with further treatment at 650°C for 1 hour, petalite ($\text{LiAlSi}_4\text{O}_{10}$, JCPDS No. 83-1470) phase appears, which has a layered structure of $\text{Si}_2\text{O}_5^{2-}$ sheets (like $\text{Li}_2\text{Si}_2\text{O}_5$) linked by Li and Al tetrahedra. A β -quartz phase (JCPDS No. 89-8949) is also observed at this thermal treatment. At 815°C for 1 hour, a small peak due to Li_3PO_4 (JCPDS No. 15-0760) is detected and β -quartz solid solution (a lithium aluminosilicate phase, β -quartz ss) appears, as evidenced by the shift of the main peak of the β -quartz phase to lower 2θ value. Petalite and Li_2SiO_3 are no more observable. With higher treatment temperature (900°C , 1 hour), β -spodumene solid solution (β -spodumene ss, JCPDS No. 35-0794) phase appears.

For the LAS0.7-P1 composition (figure 2b), the as-cast glass also shows an amorphous bump, but the crystallization sequence is different for the annealed samples. The first Bragg peak appears at 750°C for 1 minute and is attributed

175 to a β -quartz solid solution (JCPDS No. 31-0707). With further annealing at
800°C for 1 minute, peaks characteristic of β -spodumene solid solution (JCPDS
No. 35-0794) appears. Li_2SiO_3 (JCPDS No. 29-0829) and Li_3PO_4 (JCPDS No.
15-0760) crystals are observed after 1 hour treatment at 800 °C.

Raman study was performed on the two selected glass and glass-ceramic
180 compositions. No curve fitting or deconvolution of the spectra have been done,
since spectra were recorded only to get the signatures of the different amorphous
and crystalline phases. In addition, information can be obtained on the phos-
phorous environment in the glass and its evolution with temperature by looking
at the 950 cm^{-1} region, which will be detailed in the next section. Main Raman
185 peaks are assigned in figure 3.

For both glasses in figure 3(bottom), two main regions can be observed.
The region between $350\text{-}650\text{ cm}^{-1}$ is attributed mainly to bending vibrations of
Si-O and Al-O bonds associated with high-membered rings of the aluminosili-
cate network [26]. The region between $1000\text{-}1200\text{ cm}^{-1}$ is attributed to Si-O-Si,
190 Si-O-Al asymmetric stretching vibrations and symmetric Si-O⁻ stretching vi-
brations [26].

For the LAS0.2-P1 composition (figure 3a), no sharp bands are observable
before treatment at 650 °C for 1 hour. The main sharp bands at 409, 451
and 1104 cm^{-1} on the spectrum for this treatment are attributed to $\text{Li}_2\text{Si}_2\text{O}_5$
195 crystals [27]. At this temperature, crystallization of Li_2SiO_3 is also observed
by the presence of peaks at 607 and 979 cm^{-1} , close to those of pure Li_2SiO_3
(613 and 977 cm^{-1} in [28]). In addition, the band at 488 cm^{-1} , characteristic of
petalite crystals [29], is also detected at this temperature. At 740 °C for 1 hour,
the presence of a sharp band at 462 cm^{-1} indicates β -quartz crystallization [30].
200 With further annealing, at 815 °C 1 hour, the shift of the band at 462 cm^{-1} to
 479 cm^{-1} indicates the appearance of β -quartz solid solution [30]. At 900 °C 1
hour, the band is shifted to a large band near 488 cm^{-1} , characteristic of the
presence of β -spodumene solid solution (close to pure β -spodumene at 492 cm^{-1}
in [31]). The crystallization of Li_3PO_4 is evident at high temperature with the
205 sharp peak at 947 cm^{-1} close to that of pure $\gamma\text{-Li}_3\text{PO}_4$ at 950 cm^{-1} according

to [32].

For the LAS0.7-P1 composition (figure 3b), no sharp bands are observable after annealing at 750 °C 1 minute. The spectrum of heated sample at 800 °C for 1 minute shows the crystallization of β -quartz solid solution with the band at 480 cm^{-1} [30] and the shoulder at 453 cm^{-1} [31]. The apparition of β -spodumene solid solution at the expense of β -quartz solid solution is evident at 850 °C by the shift of the band from 480 to 490 cm^{-1} and by the 192 cm^{-1} band [31]. Li_3PO_4 and Li_2SiO_3 crystallization are observed after a treatment at 800 °C for 1 hour with the sharp bands at 944 cm^{-1} for Li_3PO_4 [32] and 975 and 603 cm^{-1} for Li_2SiO_3 [28].

3.1.3. Microstructure

Figure 4a shows SEM image of the LAS0.2-P1 glass treated at 650 °C for 1 minute. Small holes distributed uniformly can be observed. They are attributed to Li_2SiO_3 crystals observed on the XRD pattern, which are easily dissolved in the HF acid solution used for sample preparation, due to their low polymerization degree (chain-like structure). Figure 4b shows SEM image of the LAS0.7-P1 glass treated at 800 °C for 1 minute. Surface crystallization is visible for this sample (constituted of β -quartz ss and β -spodumene ss according to XRD pattern), while no crystal formation is detected in the bulk.

3.2. Structure of the glasses and glass-ceramics

3.2.1. Structure of as-cast glasses

The ^{31}P MAS-NMR spectra of the two glasses in figure 5a present broad resonances characteristics of the amorphous environment around phosphorous. The spectrum of LAS0.2-P1 shows a resonance at 9.2 ppm assigned to orthophosphate units (PO_4^{3-}) [33]. In addition, a second resonance around 0 ppm can be attributed to pyrophosphates units ($\text{P}_2\text{O}_7^{4-}$) [16] and possibly PO_4^{3-} species charge compensated by Al^{3+} . Indeed, replacing Li^+ by Al^{3+} , which is more strongly bonded, produces an upfield change in the chemical shift, that means more negative values [34]. In solid solution of crystallized $\text{Na}_{3-3x}\text{Al}_x\text{PO}_4$, Dol-

235 lase evidenced a change of about 8 to 9 ppm for each additional Al [34]. For
the LAS0.7-P1 composition, with a higher alumina content, a single broad reso-
nance is present at -3.5 ppm, shifted to more negative chemical shifts compared
to LAS0.2-P1, which is attributed to the presence of more Al^{3+} cations com-
pensating the PO_4^{3-} species [20]. These species containing P-O-Al bonds are
240 called POAl complexes in this study.

The ^{27}Al MAS-NMR spectra of the two glasses are shown in figure 5b.
They show a single peak in the region 55-60 ppm, ascribed to aluminum in
tetrahedral coordination (Al^{IV}). Owing to the presence of an excess of Li^+ for
the charge compensation, Al^{3+} adopts a tetrahedral conformation, as reported
245 in per-alkaline aluminosilicate glasses [35]. In addition, a small peak around
25 ppm for the LAS0.2-P1 is detected and could be due to Al^{V} as it has been
detected earlier in per-alkaline-earth aluminosilicate glasses. [36]

In order to confirm the presence of POAl complexes mentioned above in
these glasses, ^{31}P - ^{27}Al heteronuclear correlation 2D-NMR spectra have been
250 recorded to probe the spatial proximity of these nuclei [23]. For that purpose,
 $^{27}\text{Al}\{^{31}\text{P}\}$ D-HMQC spectra (figure 6) have been recorded. The two spectra
exhibit correlation signals between phosphate and aluminate species indicating
that $\text{Al}(\text{IV})\text{-PO}_4$ entities are present in the glass, even at low alumina content.
The projections of the 2D spectra are sketched as dashed lines in figure 6. They
255 show that the maximum intensity of the correlation is centered at 3.5 ppm in
the ^{31}P dimension for the LAS0.2-P1. However, this contribution does not take
into account all the information under the curve: POAl complex is not the only
entity as shown in figure 5. Two other species: PO_4^{3-} only surrounded by Li^+ at
9.2 ppm and pyrophosphate species $\text{P}_2\text{O}_7^{4-}$ around 0 ppm are observable and are
260 not affected by the correlation. For the LAS0.7-P1 composition, the maximum
is shifted to -3.5 ppm in the ^{31}P dimension. The projection of the correlation
(in dashed line on the left figure 6b) and the 1D spectrum are superimposed.
This indicates that all the P atoms are affected by the correlation and that
they see Al^{3+} atoms in their environment. This implies that all the P units are
265 connected to Al.

Previous studies on sodium aluminosilicate glasses evidenced the presence of POAl complexes [20, 21, 23]. In their study of peralkaline compositions, Toplis and Schaller [20] concluded on the presence of individual PO_4^{3-} tetrahedra linked to the aluminosilicate framework with the replacement of one or two Na atoms by Al atoms. They denoted these species $\text{Na}_2(\text{NaAl})\text{PO}_4$ and $\text{Na}(\text{NaAl})_2\text{PO}_4$ where (NaAl) represents one of the four bonds of a Al(IV) charge balanced by sodium (0.25NaAl^{4+}). $\text{Na}_2(\text{NaAl})\text{PO}_4$ is at 7 ppm while $\text{Na}(\text{NaAl})_2\text{PO}_4$ at -5 ppm. Similarly, in our peralkaline Li-aluminosilicate glasses, we can attribute the resonances at 3.5 ppm and at -3.5 ppm to $\text{Li}_2(\text{LiAl})\text{PO}_4$ and $\text{Li}(\text{LiAl})_2\text{PO}_4$, respectively. The latter species is the main contribution for the LAS0.7-P1 composition.

3.2.2. Evolution of the local environment around P with temperature

The ^{31}P MAS-NMR spectra of the glass LAS0.2-P1 and glass-ceramics show differences with thermal treatments (figure 7a). Treatment at 550 °C for 1 hour already induces some modifications of the environment around ^{31}P though this temperature is below the glass transition temperature. The intensity of the contribution near 9.2 ppm increases in intensity and its position is shifted to 9.5 ppm. On the spectrum of the sample treated at 650 °C for 1 minute, the resonance is shifted again to higher chemical shift near 10 ppm and its intensity becomes sharper, indicating the onset of orthophosphate crystallization. Indeed, the chemical shift is close to the chemical shift of pure crystalline Li_3PO_4 (10 ppm) [33]. However, the linewidth of the resonance is still large (~ 3 ppm) indicating a chemical shift distribution due to some residual disorder. The persistence of disorder suggests the presence of a poorly crystallized intermediate species. With further thermal treatments at 650 °C, 740 °C, 815 °C and 900 °C for 1 hour, this contribution becomes even sharper and its linewidth decreases to ~ 0.8 ppm at 900 °C, the same order of magnitude for the linewidth has been observed in the study of Bischoff et al. [17] at high temperature treatment. These modifications reveals the increasing crystallinity of this orthophosphate species (Li_3PO_4). In parallel, the resonances at 3.5 ppm and around 0 ppm decrease

in intensity and almost disappear at 815°C. The only resonance remaining at 900°C is the one at 10.3 ppm, corresponding to crystalline Li_3PO_4 (figure 7a). These changes are also consistent with the thermal evolution associated with P environment observed by RAMAN spectroscopy (figure 3a). The intense band
300 near 950 cm^{-1} is assigned to the symmetrical stretching vibration of the P-O bond [37]. For the as-cast glass, this band is broad and located at 957 cm^{-1} . This corresponds to P in the silicate network, mainly in orthophosphate species. With increasing annealing temperatures, the band increases in intensity and becomes sharper and its position is shifted down to 947 cm^{-1} , very close to the
305 band characteristic of $\gamma\text{-Li}_3\text{PO}_4$ located at 950 cm^{-1} [32]. The shift in position starts at 550°C for 1 hour treatment, in agreement with the evolution of the local P environment determined by NMR (figure 7a).

For the composition LAS0.7-P1, the ^{31}P MAS-NMR spectra of the glass and the glass-ceramics heat-treated at 700°C and 750°C for 1 minute are nearly
310 identical. A peak at 10 ppm attributed to nanocrystalline Li_3PO_4 (linewidth ~ 1.8 ppm) appears after a treatment at 800°C for 1 minute, while the contribution around -3.5 ppm is still present. With annealing at 800°C, 850°C and 900°C for 1 hour, this peak becomes sharper and its position is shifted to 10.6 ppm (linewidth of ~ 1.1 ppm). It is the only observable contribution at the
315 end of annealing treatments.

The RAMAN spectra for the LAS0.7-P1 composition (figure 3b) are also in agreement with the evolution observed by NMR. Unlike the LAS0.2-P1 composition, no PO_4^{3-} band is discernible at 957 cm^{-1} in the as-cast glass. The band associated with Li_3PO_4 (944 cm^{-1}) first appears after the 800°C 1 minute
320 treatment like in the NMR spectrum.

4. Discussion

4.1. Chemical dependence of the crystallization process

The DSC study provided evidence for two contrasting crystallization behaviors of the glasses, depending on their alumina contents. At low alumina

325 content, addition of P_2O_5 results in DSC peaks that become sharper and lo-
cated at lower temperatures compared to the glasses without P_2O_5 . It is known
that for a given heating rate ($10^\circ C/min$ in all our DSC experiments), a sharp
peak (small ΔT) denotes bulk crystallization while a broad peak (large ΔT) is
an indication of surface crystallization [38]. SEM analysis (figure 4b) confirms
330 mainly internal crystallization for the LAS0.2-P1 glass (figure 4a). Moreover,
the addition of efficient nucleating agents such as TiO_2 and ZrO_2 in some alu-
minosilicate glasses leads to crystallization peaks at low temperatures [39, 40].
This effect was also observed for P_2O_5 in lithium disilicate-based glass [41, 42],
which was explained by more nucleation sites created with the addition of P_2O_5 .

335 For high alumina content $R \geq 0.7$, crystallization peaks are broad with or
without P_2O_5 , suggesting surface crystallization in both cases, which is con-
firmed by SEM analysis (figure 4b). In addition, T_c is higher with P_2O_5 , re-
vealing a delay in crystallization in this glass composition. This suggests an
opposite effect of the P_2O_5 compared to the glass with low alumina content.
340 This difference of nucleation efficiency with P_2O_5 has been also evidenced in
a previous study [10]. They have observed for a compositionally complex LAS
glass with 2.5 wt% P_2O_5 that surface crystallization is favored at high alumina
content while volume crystallization is obtained at low alumina content. How-
ever, the origin of this difference has not been investigated. To understand this
345 contrasting behavior, we have considered the structural evolution of the local P
environment during different annealing treatments. As shown earlier [11] [43],
crystalline phases containing phosphate are observed by XRD only for high
temperature treatments, whereas NMR and Raman spectroscopies are able to
detect subtle variations at much lower temperature, even in the T_g range. This
350 is because XRD necessitates the organization of large crystallization domains,
whereas NMR and RAMAN investigate disordered and ordered local arrange-
ments.

4.2. P_2O_5 as nucleating agent

Upon annealing, important changes of the P environments can be observed
355 with two distinct behaviors for the low and high alumina glass compositions
(figure 7). For the LAS0.2-P1 glass, modifications of the P environment is
observed for the glass heat treated at 550 °C for 1 hour (figure 7a), i.e. prior
to the detection of any crystallization with XRD (figure 2a). This suggests
that some structural relaxation takes place, which corresponds to a structural
360 reorganization around phosphorous atoms. Raman analysis (figure 3a) confirms
this initial reorganization around P.

In the sample heat treated at 650 °C for 1 minute, the orthophosphate con-
tribution is shifted towards high chemical shift values and its intensity becomes
sharper, indicating that P atoms evolves towards an environment consistent with
365 the formation of crystalline Li_3PO_4 but not well crystallized, as the linewidth
is large compared to pure Li_3PO_4 . This species appears concomitantly with the
crystallization of the first phases detected by XRD (Li_2SiO_3 and $Li_2Si_2O_5$ in our
study). This disordered Li_3PO_4 has been suggested as an intermediate nucle-
ation step in previous crystallization investigations for non stoichiometric disil-
370 icate glasses [17][18]. In these studies, a strongly disordered P-containing phase
appears first with Li_2SiO_3 crystallization while well-ordered crystalline Li_3PO_4
appears at higher temperature together with the formation of $Li_2Si_2O_5$ [17][18].

Similarly, annealing of the LAS0.2-P1 glass at higher temperatures (650 °C
1h, 740 °C 1h and 815 °C 1h) lead to an increase of the ordering around P as indi-
375 cated by the sharpening of the NMR resonance at 10 ppm. This is accompanied
by the disappearance of the pyrophosphate $Li_4P_2O_7$ and $Li_2(LiAl)PO_4$ species.
After annealing at 900 °C for 1 hour, the only contribution is at 10.3 ppm,
attributed to well-crystallized Li_3PO_4 and Bragg peaks characteristics of this
phase are observed by XRD.

380 ^{31}P MAS-NMR spectrum for the LAS0.2-P1 glass show that the monomeric
 PO_4^{3-} and dimeric $P_2O_7^{4-}$ units are essentially present in the as-cast glass,
surrounded by Li^+ ions to ensure charge compensation of the tetrahedral units.
An ascertained role of P is to promote phase separation in glasses [9]. However,

it is difficult to conclude if the PO_4^{3-} tetrahedra are isolated from each other or
385 if they tend to segregate within the silicate network. Using an advanced NMR
technique (^{31}P spin-counting), Fayon et al. [44] have shown that nanometric-
sized heterogeneities can be evidenced in a lime phosphosilicate bioactive glass
with phosphate clusters containing 5-6 PO_4^{3-} entities. A similar approach ap-
pears unsuccessful in our glass since we have measured that the relaxation time
390 is too low (<7 ms) compared to the one (around 20 ms) required to probe P-P
connectivities with this technique.

Although the glass studied is transparent and no phase separation is observ-
able by SEM, nano-heterogeneities in terms of P-enriched nano-domains could
still be present. Indeed, Dargaud et al. [45] evidenced nano heterogeneities by
395 electron microscopy of 1-5 nm for a $\text{MgO-Al}_2\text{O}_3\text{-SiO}_2$ glass with ZrO_2 addition
though the glass is transparent and appears as amorphous by XRD. Interest-
ingly, during the first annealing treatments, the P environment evolves towards
the formation of disordered Li_3PO_4 domains. Locally, these clusters correspond
to Li^+ ions scavenged by the phosphorous atom and a remaining silicate net-
400 work depleted in Li^+ ions and, thereby, more polymerized. This is confirmed
by Bischoff et al. [17], who evidenced by a $^{29}\text{Si}/^7\text{Li}$ NMR correlation technique
a lithium clusterization before crystallization of Li_2SiO_3 . These disordered or-
thophosphate clusters embedded in the silicate network have two possible effects
on the crystallization mechanism. First, the crystallization of silicate phases is
405 possible due to lowering interfacial energy resulting from a high concentration
of Li atoms and a low polymerization of the silicate network close to Li- or-
thophosphate clusters. These compositional and structural fluctuations should
promote the formation of Li_2SiO_3 . This scenario explains the proximity of the
silicate phases and Li_3PO_4 and corresponds to the epitaxial growth observed in
410 a early study by Headley and Loehman [15]. Alternatively, the orthophosphate
heterogeneities are embedded in a silicate network whose composition is shifted
towards the center of the $\text{Li}_2\text{O-SiO}_2$ immiscibility dome. This could promote
phase separation between Li-rich regions and Si-rich regions, not necessarily
associated with the orthophosphate domains. Again, such liquid-liquid phase

415 separation could favor homogeneous nucleation of silicate phases. In both cases,
internal crystallization is achieved.

4.3. P_2O_5 as inhibitor of crystallization

In the case of the LAS0.7-P1 composition, the ^{31}P MAS-NMR spectra of
glasses annealed at 700 °C and 750 °C for 1 minute show very little variation
420 compared to the as-cast glass (figure 7b). The first important modification in
the NMR spectra appears after annealing at 800 °C for 1 minute, that is after
the first crystallization observable by XRD at 750 °C for 1 minute. At 800 °C,
a peak at 10 ppm appears due to nanocrystalline Li_3PO_4 while the contribution
 $\text{Li}(\text{LiAl})_2\text{PO}_4$ is still present. In the RAMAN spectra in figure 3b, the two first
425 modifications appear simultaneously at 800 °C: the main band characteristic of
 β -quartz ss and the one due to Li_3PO_4 . Both NMR and RAMAN agree that
no rearrangement around P is observed before crystallization of the LAS0.7-P1
glass, contrary to LAS0.2-P1. When crystallization of Li_3PO_4 occurs, POAl
complexes are no more detected in the NMR spectra.

430 In the LAS0.7-P1 composition, the nanocrystalline Li_3PO_4 appears after
crystallization of the aluminosilicate network and this is not preceded by a reor-
ganization of the P environment. This indicate that for the Al-rich compositions,
P does not play an active role in the crystallization process, which explains that
surface crystallization mainly occurs. A nucleating role for P is likely inhibited
435 by the formation of POAl complexes. Though spatial proximities between P and
Al is revealed by the $^{27}\text{Al}\{^{31}\text{P}\}$ D-HMQC correlation technique for the two com-
positions with low and high alumina content, the POAl complexes are present in
a minor amount in LAS0.2-P1 NMR spectra at 3.5 ppm. The POAl complexes
present for low alumina content strongly suggests a preferential association of
440 these two cations. For the LAS0.7-P1 glass (figure 6b), the component at-
tributed to POAl complexes is clearly predominant (at -3.5 ppm) and no PO_{43}^-
tetrahedra surrounded only by Li^+ or $\text{P}_2\text{O}_7^{4-}$ can be detected. This indicates
that addition of P_2O_5 results in the incorporation of PO_4^+ tetrahedral units
within the aluminosilicate network. Due to the Al avoidance rule, few Al-O-Al

445 bondings are expected and Al atoms are dispersed within the polymeric network
of alkali aluminosilicate glasses [46][47]. Consequently, phosphorus atoms are
likely well-separated within the aluminosilicate network due to their bonding
with Al. Such network organization prevents the formation of phosphate clus-
ters and the formation of Li-rich zones, contrary to LAS0.2-P1. Furthermore,
450 PO_4^+ sites are stabilized as charge balance is ensured by AlO_4^- tetrahedra [48].
The formation of P-O- Fe^{3+} complexes in silicate melts was also proposed to
hinder the crystallization of magnetite [49].

In addition, T_c peaks (Figure 1) appears at lower temperatures in LAS0.7-P0
compared to LAS0.7-P1 indicating that P_2O_5 mitigates the surface crystalliza-
455 tion of β -quartz ss. P_2O_5 plays no role in bulk crystallization but affects in
another way the crystallization of this glass by stabilizing the glass structure.
Others studies concluded on this dual role of P_2O_5 depending the composition
in SrO-TiO₂-Al₂O₃-SiO₂-B₂O₃ system [50]. In addition, in a Na₂O-2CaO-
3SiO₂ glass, addition of 2 wt% of P_2O_5 enhances glass-forming tendency by
460 diminishing nucleation rate[51].

5. Conclusions

Compositions from the LAS system with different $R = \frac{\text{Al}_2\text{O}_3}{\text{Li}_2\text{O}}$ ratio and with
 P_2O_5 have been investigated. Thermal analysis showed a distinct crystallization
behavior for low and high alumina content. 2 compositions were selected with
465 low and high alumina content, and phase evolution and environment around
phosphorus have been explored, as well as their modification after thermal
treatments at different temperatures. This work reveals two distinct roles of
 P_2O_5 depending on the presence of POAl complexes: easier bulk crystallization
is obtained for the R=0.2 composition, indicating a nucleating role for P_2O_5 ,
470 while higher crystallization temperatures are observed for the R=0.7 composi-
tion, suggesting that P_2O_5 enhances glass stability. The POAl complexes could
be detected even with low alumina content thanks to the enhanced sensitivity of
the D-HMQC NMR pulse sequence. The nucleating role of P_2O_5 is not related

to the crystallization of lithium orthophosphate phases, as these crystals appears
475 after the crystallization of lithium silicate phases. The presence, and develop-
ment upon annealing, of structurally disordered heterogeneities associated with
P is responsible for changes in structure and properties of the remaining glass,
which promotes crystallization at low alumina content. With increasing Al_2O_3
content, the POAl complexes become the dominant species. These complexes
480 result in the dispersion of phosphate species within the glass matrix and prevent
the formation of the heterogeneities associated with P. As a consequence, P_2O_5
can be considered as a crystallization inhibitor in LAS glasses with high alumina
content.

Acknowledgments

485 We would like to acknowledge Anne Crochet (CETC Corning) for SEM
images, Peggy Georges and Sandrine Bercy (CETC Corning) for chemical anal-
ysis. We thank also Laurent Delevoye for fruitful discussions. The ANRT is
acknowledged for PhD funding (P.G.) under the CIFRE Contract 2015/0529.
The authors thank the Chevreul Institute (FR 2638) for its help in the devel-
490 opment of this work. Chevreul Institute is supported by the « Ministère de
l'Enseignement Supérieur et de la Recherche », the « Région Nord-Pas de calais
» and the « Fonds Européen de Développement des Régions ».

References

- [1] W. Höland, G. H. Beall, Glass-ceramics technology, Wiley-American Ce-
495 ramic Society, 2012.
- [2] G. H. Beall, L. R. Pinckney, Nanophase glass-ceramics, J. Am. Ceram.
Soc. 82 (1) (1999) 5–16.
URL <http://onlinelibrary.wiley.com/doi/10.1111/j.1151-2916.1999.tb01716.x/full>

- 500 [3] M. Comte, Commercial applications of glass-ceramics, in: From glass to
crystal, EDP Sciences, 2017, pp. 361–374.
- [4] S. Huang, Y. Li, S. Wei, Z. Huang, W. Gao, P. Cao, A novel high-
strength lithium disilicate glass-ceramic featuring a highly inter-
twined microstructure, *J. Eur. Ceram. Soc* 37 (3) (2016) 1083–1094.
505 doi:10.1016/j.jeurceramsoc.2016.10.020.
URL [http://linkinghub.elsevier.com/retrieve/pii/
S0955221916305702](http://linkinghub.elsevier.com/retrieve/pii/S0955221916305702)
- [5] W. Holand, V. Rheinberger, M. Schweiger, Control of nucleation in glass
ceramics, *Philos. Trans. R. Soc. London, Ser. A* 361 (1804) (2003) 575–589.
510 doi:10.1098/rsta.2002.1152.
URL [http://rsta.royalsocietypublishing.org/cgi/doi/10.1098/
rsta.2002.1152](http://rsta.royalsocietypublishing.org/cgi/doi/10.1098/rsta.2002.1152)
- [6] L. R. Pinckney, G. H. Beall, Microstructural evolution in some silicate
glass-ceramics: A review, *J. Am. Ceram. Soc.* 91 (3) (2008) 773–779. doi:
515 10.1111/j.1551-2916.2007.02129.x.
URL <http://doi.wiley.com/10.1111/j.1551-2916.2007.02129.x>
- [7] E. D. Zanotto, V. M. Fokin, Recent studies of internal and surface
nucleation in silicate glasses, *Philos. Trans. R. Soc. Lond. A* 361 (1804)
(2003) 591–613. doi:10.1098/rsta.2002.1150.
520 URL [http://rsta.royalsocietypublishing.org/cgi/doi/10.1098/
rsta.2002.1150](http://rsta.royalsocietypublishing.org/cgi/doi/10.1098/rsta.2002.1150)
- [8] M. J. Toplis, D. B. Dingwell, The variable influence of P_2O_5 on the viscosity
of melts of differing alkali/aluminium ratio: Implications for the structural
role of phosphorus in silicate melts, *Geochim. Cosmochim. Acta* 60 (21)
525 (1996) 4107–4121.
- [9] P. F. James, Liquid-phase separation in glass-forming systems, *J. Mater.
Sci.* 10 (10) (1975) 1802–1825.
URL <http://link.springer.com/article/10.1007/BF00554944>

- [10] A. Arvind, A. K. Tyagi, R. Mishra, V. K. Shrikhande, G. P. Kothiyal,
530 Evolution of crystalline phases as a function of composition and dwell time
in lithium aluminium silicate glass-ceramics, *Phys. Chem. Glasses-Eur. J.*
Glass Sci. Technol. B 49 (3) (2008) 166–173.
- [11] W. Höland, E. Apel, C. van't Hoen, V. Rheinberger, Stud-
ies of crystal phase formations in high-strength lithium disilicate
535 glass-ceramics, *J. Non-Cryst. Solids* 352 (38) (2006) 4041–4050.
doi:10.1016/j.jnoncrysol.2006.06.039.
URL [http://linkinghub.elsevier.com/retrieve/pii/
S0022309306010052](http://linkinghub.elsevier.com/retrieve/pii/S0022309306010052)
- [12] X. Zheng, G. Wen, L. Song, X. Huang, Effects of P_2O_5 and
540 heat treatment on crystallization and microstructure in lithium
disilicate glass ceramics, *Acta Mater.* 56 (3) (2008) 549–558.
doi:10.1016/j.actamat.2007.10.024.
URL [http://linkinghub.elsevier.com/retrieve/pii/
S1359645407006933](http://linkinghub.elsevier.com/retrieve/pii/S1359645407006933)
- 545 [13] F. Wang, J. Gao, H. Wang, J.-h. Chen, Flexural strength and
translucent characteristics of lithium disilicate glass-ceramics with
different P_2O_5 content, *Mater. Design* 31 (7) (2010) 3270–3274.
doi:10.1016/j.matdes.2010.02.013.
URL [http://linkinghub.elsevier.com/retrieve/pii/
550 S0261306910000865](http://linkinghub.elsevier.com/retrieve/pii/S0261306910000865)
- [14] S. C. von Clausbruch, M. Schweiger, W. Höland, V. Rheinberger, The
effect of P_2O_5 on the crystallization and microstructure of glass-ceramics
in the SiO_2 – Li_2O – K_2O – ZnO – P_2O_5 system, *J. Non-Cryst. Solids* 263–264
(2000) 388–394. doi:10.1016/S0022-3093(99)00647-X.
555 URL [http://www.sciencedirect.com/science/article/pii/
S002230939900647X](http://www.sciencedirect.com/science/article/pii/S002230939900647X)
- [15] T. J. Headley, R. E. Loehman, Crystallization of a glass-ceramic by

- epitaxial growth, *J. Am. Chem. Soc.* 67 (9) (1984) 620–625.
URL <http://onlinelibrary.wiley.com/doi/10.1111/j.1151-2916.1984.tb19606.x/full>
560
- [16] D. Holland, Y. Iqbal, P. James, B. Lee, Early stages of crystallisation of lithium disilicate glasses containing P_2O_5 - An NMR study, *J. Non-Cryst. Solids* 232-234 (1998) 140–146. doi:[http://dx.doi.org/10.1016/S0022-3093\(98\)00381-0](http://dx.doi.org/10.1016/S0022-3093(98)00381-0).
565 URL <http://www.sciencedirect.com/science/article/pii/S0022309398003810>
- [17] C. Bischoff, H. Eckert, E. Apel, V. M. Rheinberger, W. Höland, Phase evolution in lithium disilicate glass-ceramics based on non-stoichiometric compositions of a multi-component system: structural studies by ^{29}Si single and double resonance solid state NMR, *Phys. Chem. Chem. Phys.* 13 (10)
570 (2011) 4540–4551. doi:10.1039/c0cp01440k.
- [18] S. Huang, Z. Zujovic, Z. Huang, W. Gao, P. Cao, Crystallization of a high-strength lithium disilicate glass-ceramic: An XRD and solid-state NMR investigation, *J. Non-Cryst. Solids* 457 (2017) 65–72. doi:10.1016/j.jnoncrysol.2016.11.015.
575
- [19] A. Ananthanarayanan, G. Tricot, G. P. Kothiyal, L. Montagne, A comparative overview of glass-ceramic characterization by MAS-NMR and XRD, *Crit. Rev. Solid State Mater. Sci.* 36 (4) (2011) 229–241. doi:10.1080/10408436.2011.593643.
580 URL <http://www.tandfonline.com/doi/abs/10.1080/10408436.2011.593643>
- [20] M. J. Toplis, T. Schaller, ^{31}P MAS NMR study of glasses in the system $xNa_2O-(1-x)Al_2O_3-2SiO_2-yP_2O_5$, *J. Non-Cryst. Solids* 224 (1) (1998) 57–68. doi:10.1016/S0022-3093(97)00458-4.
- 585 [21] T. Schaller, C. Rong, M. J. Toplis, H. Cho, TRAPDOR NMR investigations of phosphorus-bearing aluminosilicate glasses, *J. Non-Cryst. Solids*

248 (1) (1999) 19–27.

URL <http://www.sciencedirect.com/science/article/pii/S0022309399000988>

- 590 [22] J. Trebosc, B. Hu, J. Amoureux, Z. Gan, Through-space R^3 -HETCOR experiments between spin-1/2 and half-integer quadrupolar nuclei in solid-state NMR, *J. Magn. Reson.* 186 (2) (2007) 220–227. doi:10.1016/j.jmr.2007.02.015.

URL <http://linkinghub.elsevier.com/retrieve/pii/S1090780707000699>

- 595 [23] G. Tricot, O. Lafon, J. Trebosc, L. Delevoye, F. Méar, L. Montagne, J.-P. Amoureux, Structural characterisation of phosphate materials: new insights into the spatial proximities between phosphorus and quadrupolar nuclei using the D-HMQC MAS NMR technique, *Phys. Chem. Chem. Phys.* 13 (37) (2011) 16786–16794. doi:10.1039/c1cp20993k.

- [24] D. Massiot, F. Fayon, M. Capron, I. King, S. Le Calvé, B. Alonso, J.-O. Durand, B. Bujoli, Z. Gan, G. Hoatson, Modelling one-and two-dimensional solid-state NMR spectra, *Magn. Reson. Chem.* 40 (1) (2002) 70–76. doi:10.1002/mrc.984.

- 605 [25] M. L. Nascimento, L. A. Souza, E. B. Ferreira, E. D. Zanotto, Can glass stability parameters infer glass forming ability?, *J. Non-Cryst. Solids* 351 (40) (2005) 3296–3308. doi:10.1016/j.jnoncrysol.2005.08.013.

URL <http://linkinghub.elsevier.com/retrieve/pii/S002230930500623X>

- 610 [26] A. K. Yadav, P. Singh, A review of the structures of oxide glasses by Raman spectroscopy, *RSC Adv.* 5 (83) (2015) 67583–67609. doi:10.1039/C5RA13043C.

URL <http://xlink.rsc.org/?DOI=C5RA13043C>

- [27] T. Fuss, A. Mognuš-Milanković, C. S. Ray, C. Lesher, R. Youngman, D. E.

- 615 Day, Ex situ XRD, TEM, IR, Raman and NMR spectroscopy of crystal-
lization of lithium disilicate glass at high pressure, *J. Non-Cryst. Solids*
352 (38) (2006) 4101–4111. doi:10.1016/j.jnoncrysol.2006.06.038.
URL [http://linkinghub.elsevier.com/retrieve/pii/
S0022309306009513](http://linkinghub.elsevier.com/retrieve/pii/S0022309306009513)
- 620 [28] P. Richet, B. O. Mysen, D. Andrault, Melting and premelting of silicates:
Raman spectroscopy and X-ray diffraction of Li_2SiO_3 and Na_2SiO_3 , *Phys.*
Chem. Miner. 23 (3) (1996) 157–172.
- [29] A. A. Kaminskii, E. Haussühl, H. J. Eichler, J. Hanuza, M. Maćzka,
H. Yoneda, A. Shirakawa, Lithium silicate, $\text{LiAlSi}_4\text{O}_{10}$ (petalite) - a novel
625 monoclinic SRS-active crystal, *Laser Phys. Lett.* 12 (8) (2015) 085002.
doi:10.1088/1612-2011/12/8/085002.
URL [http://stacks.iop.org/1612-202X/12/i=8/a=085002?key=
crossref.4d712c851a779614673482a03e16af7f](http://stacks.iop.org/1612-202X/12/i=8/a=085002?key=crossref.4d712c851a779614673482a03e16af7f)
- [30] I. Alekseeva, O. Dymshits, V. Ermakov, A. Zhilin, V. Petrov,
630 M. Tsenter, Raman spectroscopy quantifying the composition
of stuffed β -quartz derivative phases in lithium aluminosilicate
glass-ceramics, *J. Non-Cryst. Solids* 354 (45) (2008) 4932–4939.
doi:10.1016/j.jnoncrysol.2008.07.016.
URL [http://linkinghub.elsevier.com/retrieve/pii/
635 S0022309308005449](http://linkinghub.elsevier.com/retrieve/pii/S0022309308005449)
- [31] S. Sharma, B. Simons, Raman-study of crystalline polymorphs and glasses
of spodumene composition quenched from various pressures, *Am. Miner.*
66 (1) (1981) 118–126.
- [32] L. Popović, B. Manoun, D. de Waal, M. K. Nieuwoudt, J. D. Comins, Ra-
640 man spectroscopic study of phase transitions in Li_3PO_4 , *J. Raman Spec-*
trosc. 34 (1) (2003) 77–83. doi:10.1002/jrs.954.
URL <http://doi.wiley.com/10.1002/jrs.954>

- [33] R. Dupree, D. Holland, M. G. Mortuza, The role of small amounts of P_2O_5 in the structure of alkali disilicate glasses, *Phys. Chem. Glasses* 29 (1) (1988) 18–21.
- 645
- [34] W. A. Dollase, L. H. Merwin, A. Sebald, Structure of $Na_{3-3x}Al_xPO_4$, $x=0$ to 0.5, *J. Solid State Chem.* 83 (1989) 140–149.
- [35] J. F. Stebbins, S. Kroeker, S. K. Lee, T. J. Kiczanski, Quantification of five- and six-coordinated aluminum ions in aluminosilicate and fluoride-containing glasses by high-field, high-resolution ^{27}Al NMR, *J. Non-Cryst. Solids* 275 (1) (2000) 1–6. doi:[http://dx.doi.org/10.1016/S0022-3093\(00\)00270-2](http://dx.doi.org/10.1016/S0022-3093(00)00270-2).
URL <http://www.sciencedirect.com/science/article/pii/S0022309300002702>
- 650
- [36] D. Neuville, L. Cormier, V. Montouillout, D. Massiot, Local Al site distribution in aluminosilicate glasses by ^{27}Al MQMAS NMR, *J. Non-Cryst. Solids* 353 (2) (2007) 180–184. doi:10.1016/j.jnoncrysol.2006.09.035.
URL <http://linkinghub.elsevier.com/retrieve/pii/S002230930601146X>
- 655
- [37] F. Harbach, F. Fischer, Raman Spectra and Optical Absorption Edge of Li_3PO_4 Single Crystals, *Phys. Status Solidi B* 66 (1) (1974) 237–245.
- [38] C. S. Ray, D. E. Day, Determining the Nucleation Rate Curve for Lithium Disilicate Glass by Differential Thermal Analysis, *J. Am. Ceram. Soc.* 73 (2) (1990) 439–442. doi:10.1111/j.1151-2916.1990.tb06532.x.
- 660
- [39] G. A. Khater, M. H. Idris, Role of TiO_2 and ZrO_2 on crystallizing phases and microstructure in Li, Ba aluminosilicate glass, *Ceramics International* 33 (2) (2007) 233–238. doi:10.1016/j.ceramint.2005.08.016.
URL <http://linkinghub.elsevier.com/retrieve/pii/S0272884205002701>
- 665

- 670 [40] L. Cormier, O. Dargaud, G. Calas, C. Jousseume, S. Papin,
N. Trcera, A. Cognigni, Zr environment and nucleation role in
aluminosilicate glasses, *Mater. Chem. Phys.* 152 (2015) 41–47.
doi:10.1016/j.matchemphys.2014.12.008.
URL [http://linkinghub.elsevier.com/retrieve/pii/
675 S0254058414007998](http://linkinghub.elsevier.com/retrieve/pii/S0254058414007998)
- [41] H. R. Fernandes, D. U. Tulyaganov, J. M. F. Ferreira, The role of P₂O₅,
TiO₂ and ZrO₂ as nucleating agents on microstructure and crystallization
behaviour of lithium disilicate-based glass, *J Mater Sci* 48 (2) (2013) 765–
773. doi:10.1007/s10853-012-6793-4.
680 URL <http://link.springer.com/10.1007/s10853-012-6793-4>
- [42] A. Gaddam, H. R. Fernandes, D. U. Tulyaganov, M. J. Ribeiro,
J. M. F. Ferreira, The roles of P₂O₅ and SiO₂/Li₂O ratio on the
network structure and crystallization kinetics of non-stoichiometric
lithium disilicate based glasses, *J. Non-Cryst. Solids* 481 (2018) 512–521.
685 doi:10.1016/j.jnoncrysol.2017.11.034.
URL [http://linkinghub.elsevier.com/retrieve/pii/
S0022309317306361](http://linkinghub.elsevier.com/retrieve/pii/S0022309317306361)
- [43] A. Ananthanarayanan, G. P. Kothiyal, L. Montagne, B. Revel, MAS-NMR
investigations of the crystallization behaviour of lithium aluminum silicate
690 (LAS) glasses containing P₂O₅ and TiO₂ nucleants, *J. Solid State Chem.*
183 (6) (2010) 1416–1422. doi:10.1016/j.jssc.2010.04.011.
URL [http://linkinghub.elsevier.com/retrieve/pii/
S0022459610001441](http://linkinghub.elsevier.com/retrieve/pii/S0022459610001441)
- [44] F. Fayon, C. Duée, T. Poumeyrol, M. Allix, D. Massiot, Evidence of
695 Nanometric-Sized Phosphate Clusters in Bioactive Glasses As Revealed
by Solid-State ³¹P-NMR, *J. Phys. Chem. C* 117 (5) (2013) 2283–2288.
doi:10.1021/jp312263j.
URL <http://pubs.acs.org/doi/abs/10.1021/jp312263j>

- [45] O. Dargaud, L. Cormier, N. Menguy, G. Patriarche, Multi-scale struc-
700 turation of glasses: Observations of phase separation and nanoscale
heterogeneities in glasses by Z-contrast scanning electron transmis-
sion microscopy, *J. Non-Cryst. Solids* 358 (10) (2012) 1257–1262.
doi:10.1016/j.jnoncrysol.2012.02.026.
URL [http://linkinghub.elsevier.com/retrieve/pii/
705 S0022309312001196](http://linkinghub.elsevier.com/retrieve/pii/S0022309312001196)
- [46] S. K. Lee, J. F. Stebbins, Al–O–Al and Si–O–Si sites in framework alumi-
nosilicate glasses with Si/Al= 1: quantification of framework disorder, *J.*
Non-Cryst. Solids 270 (1) (2000) 260–264. doi:10.1016/S0022-3093(00)
00089-2.
- 710 [47] Extent of intermixing among framework units in silicate glasses and
meltsdoi:10.1016/S0016-7037(01)00775-X.
- [48] S. Wegner, L. van Wüllen, G. Tricot, The structure of alu-
minophosphate glasses revisited: Application of modern solid state
NMR strategies to determine structural motifs on intermediate
715 length scales, *J. Non-Cryst. Solids* 354 (15-16) (2008) 1703–1714.
doi:10.1016/j.jnoncrysol.2007.10.034.
URL [http://linkinghub.elsevier.com/retrieve/pii/
S0022309307012458](http://linkinghub.elsevier.com/retrieve/pii/S0022309307012458)
- [49] M. Toplis, G. Libourel, M. Carroll, The role of phosphorus in crystallization
720 processes of basalt - an experimental study, *Geochim. Cosmochim. Acta*
58 (2) (1994) 797–810. doi:10.1016/0016-7037(94)90506-1.
- [50] M. Bengisu, R. K. Brow, A. Wittenauer, Glasses and glass-ceramics in the
SrO–TiO₂–Al₂O₃–SiO₂–B₂O₃ system and the effect of P₂O₅ additions,
J Mater Sci 43 (10) (2008) 3531–3538. doi:10.1007/s10853-008-2541-1.
725 URL <http://link.springer.com/10.1007/s10853-008-2541-1>
- [51] C. S. Ray, D. E. Day, An Analysis of Nucleation-Rate Type of Curves in
Glass as Determined by Differential Thermal Analysis, *J. Am. Ceram. Soc*

80 (12) (1997) 3100–3108.

URL <http://onlinelibrary.wiley.com/doi/10.1111/j.1151-2916.1997.tb03238.x/full>

730

Figures

Glass	SiO ₂	Al ₂ O ₃	Li ₂ O	P ₂ O ₅	R	T _g (°C)	T _x (°C)	T _c (°C)	T _x -T _g (°C)
LAS0-P0	74.4	0.3	25.3	0.01	0.01	483	659	764	176
LAS0-P1	73.6	0.2	25.1	1.1	0.01	477	606	635	129
LAS0.2-P0	75.7	4.6	19.7	0.02	0.23	507	660	832	153
LAS0.2-P1	74.3	4.2	20.7	0.8	0.20	509	592	646	83
LAS0.4-P0	74.5	7.4	18.1	0.01	0.41	536	651	770	115
LAS0.4-P1	75.0	7.6	16.4	1.0	0.46	548	617	639	69
LAS0.7-P0	73.6	10.8	15.6	0.01	0.69	594	559	769	65
LAS0.7-P1	73.8	10.2	15.0	1.0	0.68	614	708	840	94
LAS1-P0	74.0	13.2	12.8	0.003	1.03	748	852	922	104
LAS1-P1	73.7	13.0	12.5	0.79	1.04	736	936	1005	200
LAS1.3-P0	74.1	14.7	11.2	0.01	1.32	770	1080	1222	310
LAS1.3-P1	75.0	14.6	9.4	0.96	1.55	778	/	1234	/

Table 1: Compositions (mol%) analyzed by EPMA and FAES for the glasses investigated in this study. $R = \frac{Al_2O_3}{Li_2O}$. T_g is the glass transition temperature and T_x is the temperature of the first crystallization peak determined from the DSC curves. The error in the determination of T_g, T_x and T_c is estimated close to ± 2 °C.

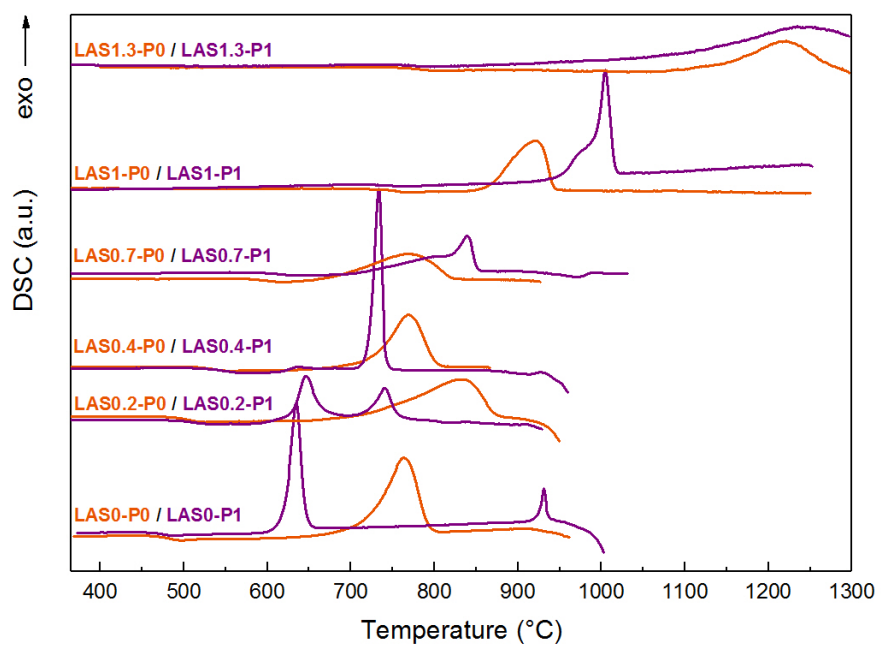
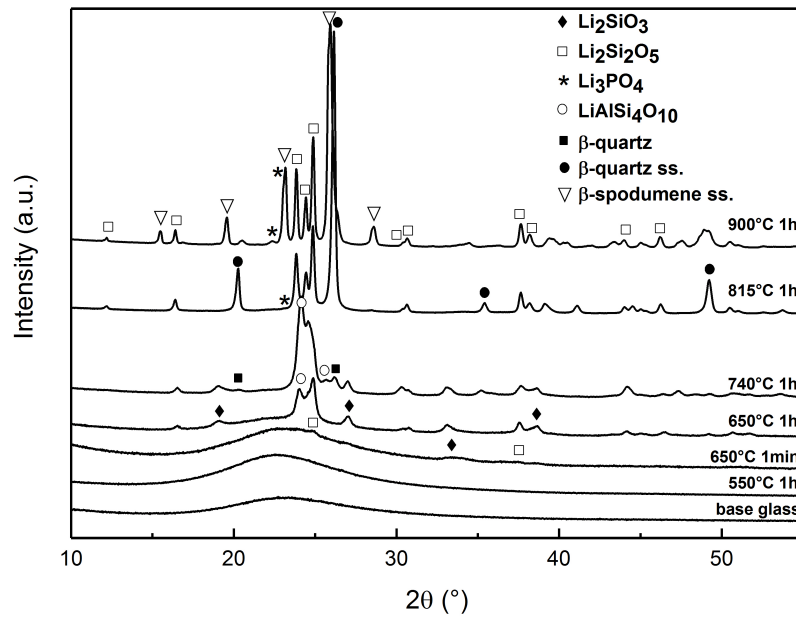
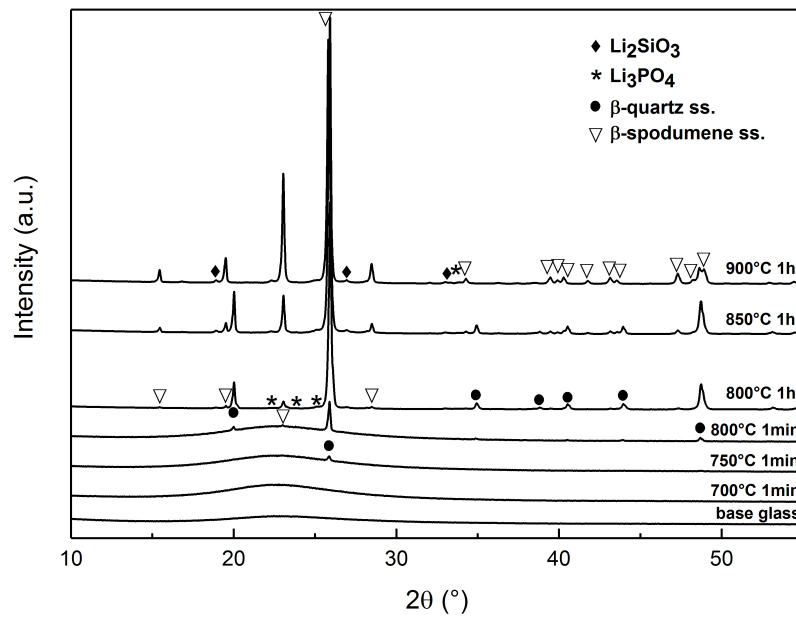


Figure 1: Differential scanning calorimetry curves of the glasses without (orange) P₂O₅ and with (purple) 1 mol% P₂O₅

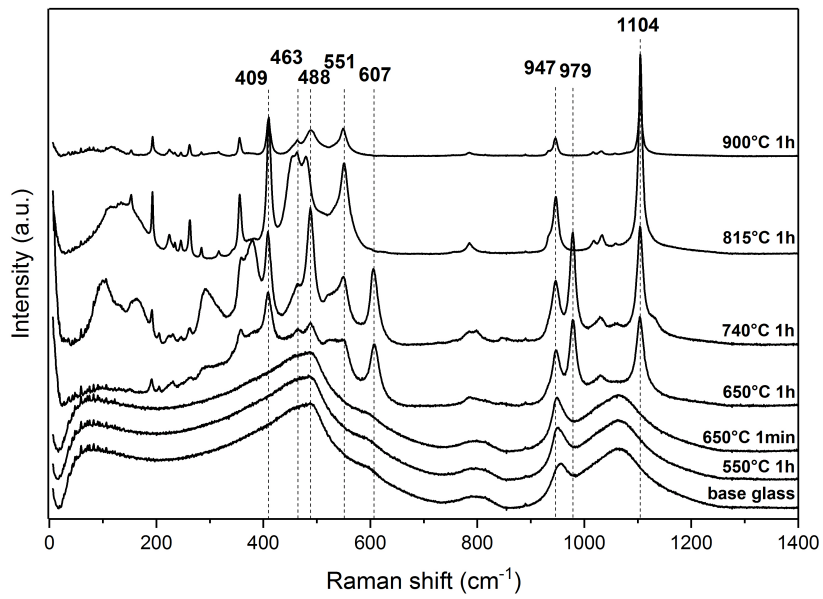


(a)

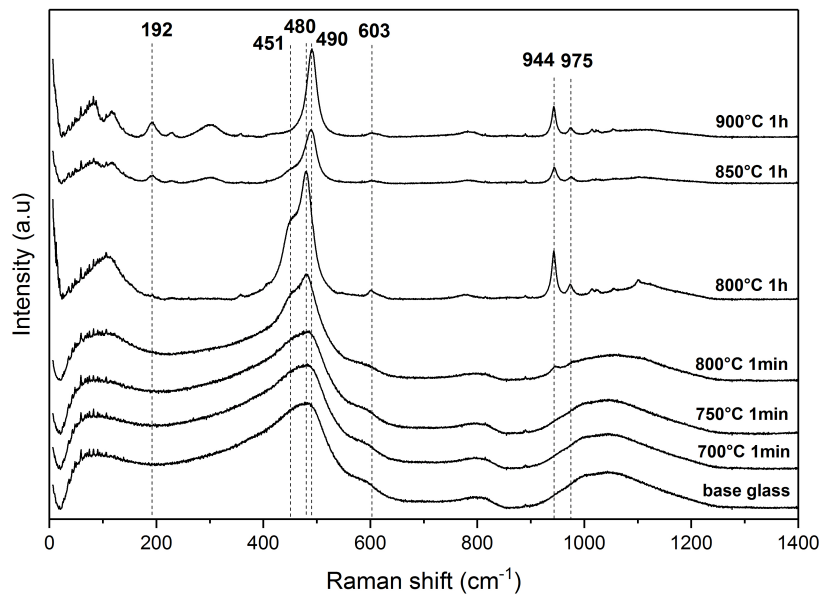


(b)

Figure 2: XRD patterns of the compositions LAS0.2-P1 (a) and LAS0.7-P1 (b) annealing at different temperatures and times

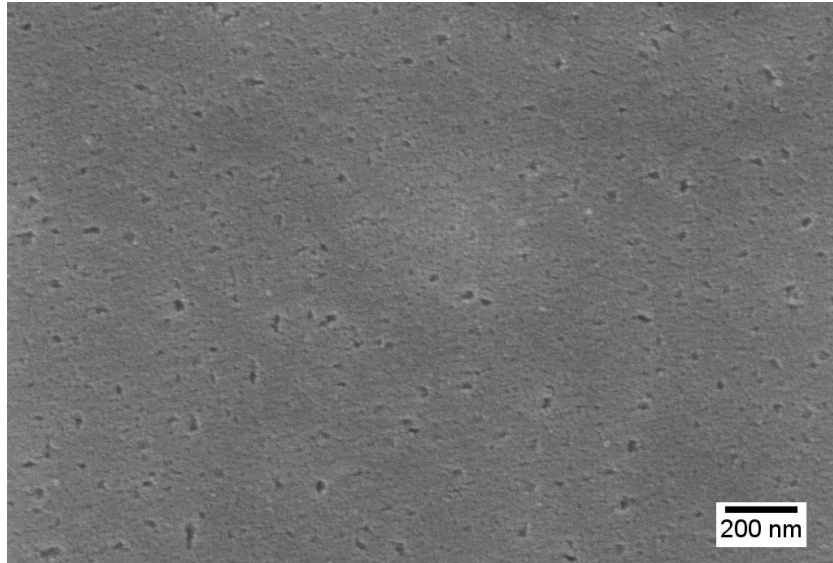


(a)

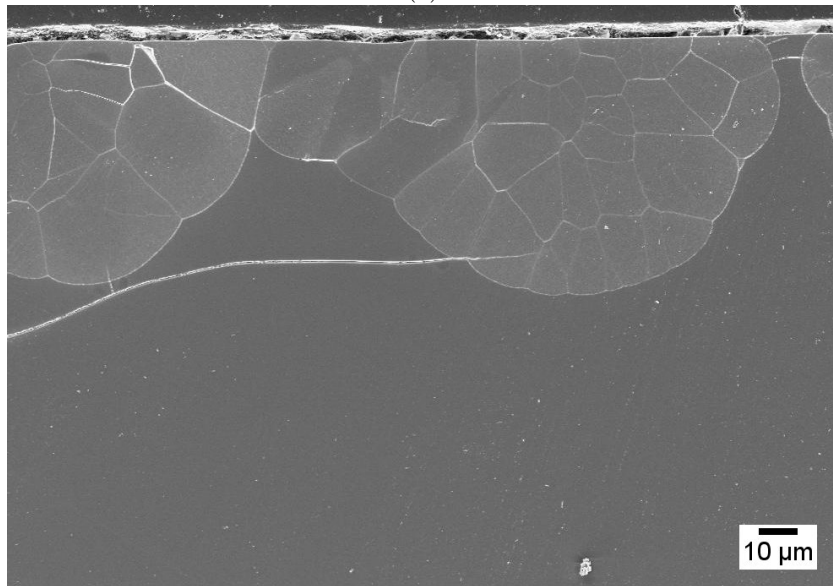


(b)

Figure 3: RAMAN spectra of LAS0.2-P1 (a) and LAS0.7-P1 (b) annealed at different temperatures and times

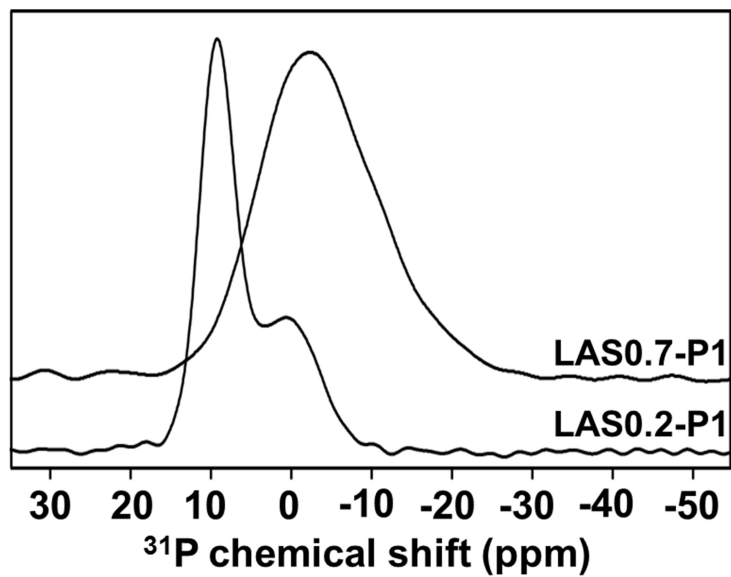


(a)

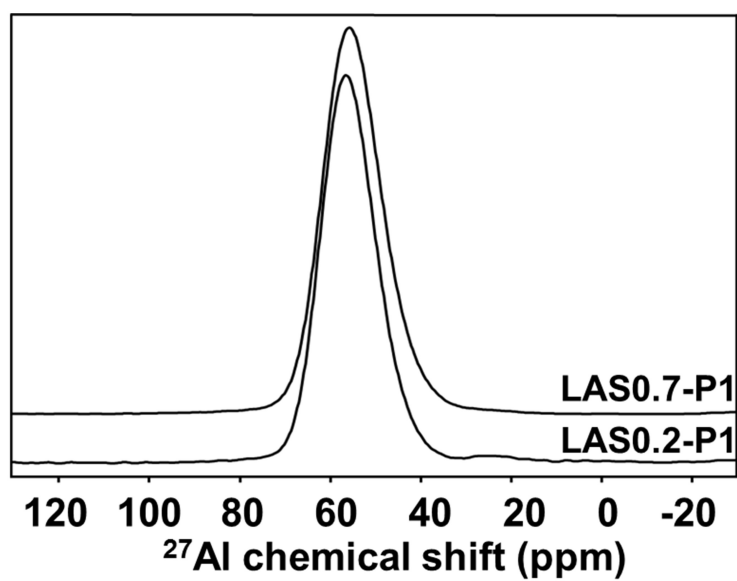


(b)

Figure 4: SEM image of samples polished then etched with 1% HF for 30 seconds of (a) LAS0.2-P1 annealed at 650 °C for 1 minute, (b) LAS0.7-P1 annealed at 800 °C for 1 minute

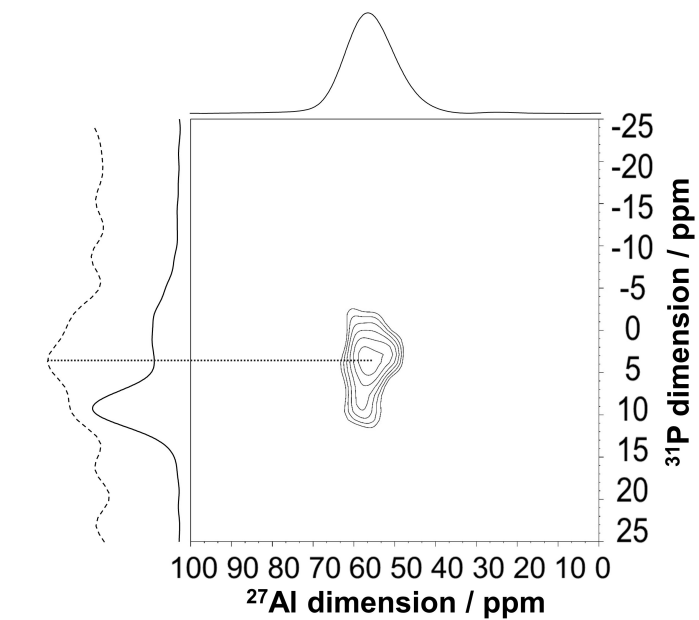


(a)

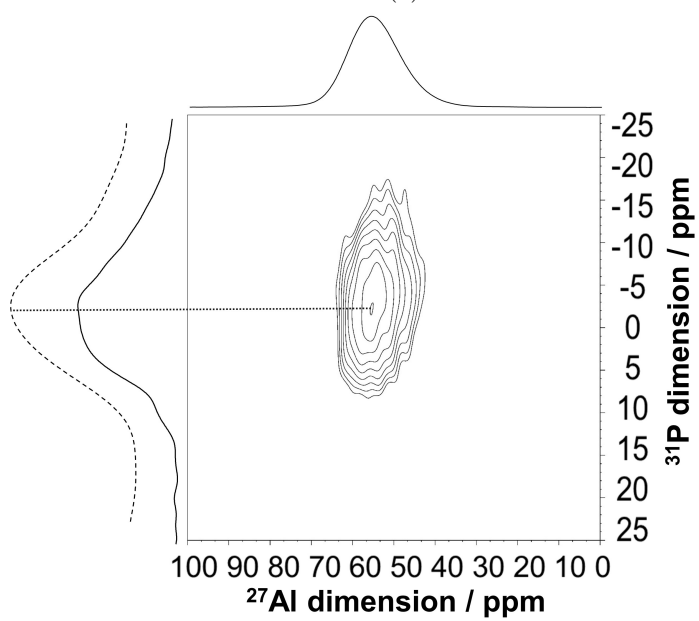


(b)

Figure 5: (a) ^{31}P MAS-NMR spectra recorded at 9.4 T, (b) ^{27}Al MAS-NMR spectra recorded at 18.8 T of as-cast glasses LAS0.2-P1 and LAS0.7-P1

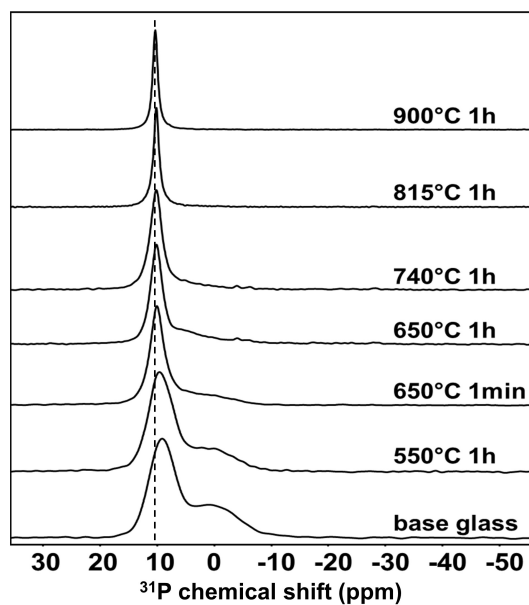


(a)

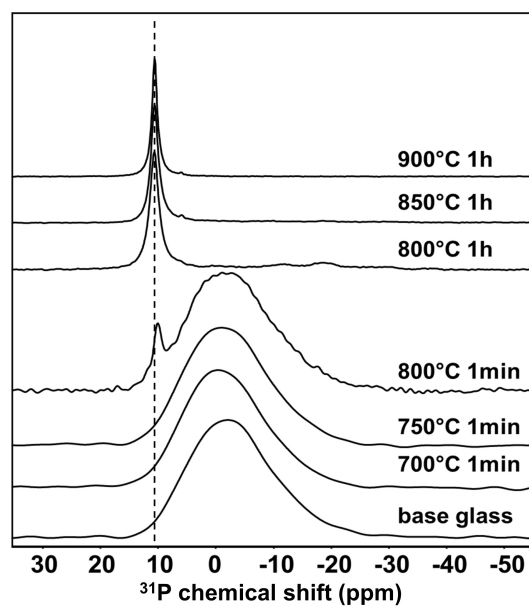


(b)

Figure 6: $^{27}\text{Al}\{^{31}\text{P}\}$ D-HMQC spectra recorded at 18.8 T of as-cast glasses LAS0.2P1 (a) and LAS0.7-P1 (b). The dashed lines are the ^{31}P projections of the 2D spectra.



(a)



(b)

Figure 7: ^{31}P MAS-NMR spectra recorded at 9.4 T of LAS0.2-P1 (a) and LAS0.7-P1 (b) annealed at different temperatures and times